Supplementary information for
"Explosive rigidity percolation in origami"

Rongxuan Li, Gary P. T. Choi

Contents

S1 Construction of the infinitesimal rigidity matrix

In the main text, we provided the explicit formulas for the partial derivatives of each edge constraint in the infinitesimal rigidity matrix A. Here, we give the explicit formulas for the partial derivatives of the other constraints in A.

For each diagonal (no-shear) constraint, suppose $\mathbf{v}_{i_3} = (x_{i_3}, y_{i_3}, z_{i_3})$ and $\mathbf{v}_{i_1} = (x_{i_1}, y_{i_1}, z_{i_1})$. We can explicitly derive the partial derivatives of g_d as follows:

$$\frac{\partial g_d}{\partial x_{i_3}} = -\frac{\partial g_d}{\partial x_{i_1}} = 2(x_{i_3} - x_{i_1}), \tag{S1}$$

$$\frac{\partial g_d}{\partial y_{i_3}} = -\frac{\partial g_d}{\partial y_{j_1}} = 2(y_{i_3} - y_{i_1}), \tag{S2}$$

$$\frac{\partial g_d}{\partial z_{i_3}} = -\frac{\partial g_d}{\partial z_{i_1}} = 2(z_{i_3} - z_{i_1}), \tag{S3}$$

and the partial derivatives of g_d with respect to all other variables are 0. This shows that each row of A associated with a diagonal constraint has at most 6 non-zero entries.

Lastly, for each quad planarity constraint added to the system, suppose $\mathbf{v}_{i_j} = (x_{i_j}, y_{i_j}, z_{i_j})$ where $j = 1, 2, 3, 4$. We can explicitly derive the partial derivatives of g_p as follows:

$$\begin{aligned}\frac{\partial g_p}{\partial x_{i_1}} = &-(y_{i_2} - y_{i_1})(z_{i_4} - z_{i_1}) + (y_{i_4} - y_{i_1})(z_{i_2} - z_{i_1}) + (y_{i_3} - y_{i_1})(z_{i_4} - z_{i_1}) \\ &-(y_{i_4} - y_{i_1})(z_{i_3} - z_{i_1}) - (y_{i_3} - y_{i_1})(z_{i_2} - z_{i_1}) + (y_{i_2} - y_{i_1})(z_{i_3} - z_{i_1}),\end{aligned} \tag{S4}$$

$$\begin{aligned}\frac{\partial g_p}{\partial y_{i_1}} = &(x_{i_2} - x_{i_1})(z_{i_4} - z_{i_1}) - (x_{i_4} - x_{i_1})(z_{i_2} - z_{i_1}) - (x_{i_3} - x_{i_1})(z_{i_4} - z_{i_1}) \\ &+(x_{i_4} - x_{i_1})(z_{i_3} - z_{i_1}) + (x_{i_3} - x_{i_1})(z_{i_2} - z_{i_1}) - (x_{i_2} - x_{i_1})(z_{i_3} - z_{i_1}),\end{aligned} \tag{S5}$$

$$\begin{aligned}\frac{\partial g_p}{\partial z_{i_1}} = &-(x_{i_2} - x_{i_1})(y_{i_4} - y_{i_1}) + (x_{i_4} - x_{i_1})(y_{i_2} - y_{i_1}) + (x_{i_3} - x_{i_1})(y_{i_4} - y_{i_1}) \\ &-(x_{i_4} - x_{i_1})(y_{i_3} - y_{i_1}) - (x_{i_3} - x_{i_1})(y_{i_2} - y_{i_1}) + (x_{i_2} - x_{i_1})(y_{i_3} - y_{i_1}),\end{aligned} \tag{S6}$$

$$\frac{\partial g_p}{\partial x_{i_2}} = -(y_{i_3} - y_{i_1})(z_{i_4} - z_{i_1}) + (y_{i_4} - y_{i_1})(z_{i_3} - z_{i_1}), \tag{S7}$$

$$\frac{\partial g_p}{\partial y_{i_2}} = (x_{i_3} - x_{i_1})(z_{i_4} - z_{i_1}) - (x_{i_4} - x_{i_1})(z_{i_3} - z_{i_1}), \tag{S8}$$

$$\frac{\partial g_p}{\partial z_{i_2}} = -(x_{i_3} - x_{i_1})(y_{i_4} - y_{i_1}) + (x_{i_4} - x_{i_1})(y_{i_3} - y_{i_1}), \tag{S9}$$

$$\frac{\partial g_p}{\partial x_{i_3}} = (y_{i_2} - y_{i_1})(z_{i_4} - z_{i_1}) - (y_{i_4} - y_{i_1})(z_{i_2} - z_{i_1}), \tag{S10}$$

$$\frac{\partial g_p}{\partial y_{i_3}} = (x_{i_4} - x_{i_1})(z_{i_2} - z_{i_1}) - (x_{i_2} - x_{i_1})(z_{i_4} - z_{i_1}), \tag{S11}$$

$$\frac{\partial g_p}{\partial z_{i_3}} = (x_{i_2} - x_{i_1})(y_{i_4} - y_{i_1}) - (x_{i_4} - x_{i_1})(y_{i_2} - y_{i_1}), \tag{S12}$$

$$\frac{\partial g_p}{\partial x_{i_4}} = (y_{i_3} - y_{i_1})(z_{i_2} - z_{i_1}) - (y_{i_2} - y_{i_1})(z_{i_3} - z_{i_1}), \tag{S13}$$

$$\frac{\partial g_p}{\partial y_{i_4}} = -(x_{i_3} - x_{i_1})(z_{i_2} - z_{i_1}) + (x_{i_2} - x_{i_1})(z_{i_3} - z_{i_1}), \tag{S14}$$

$$\frac{\partial g_p}{\partial z_{i_4}} = (x_{i_3} - x_{i_1})(y_{i_2} - y_{i_1}) - (x_{i_2} - x_{i_1})(y_{i_3} - y_{i_1}), \tag{S15}$$

and the partial derivatives of g_p with respect to all other variables are 0. This shows that each row of A associated with a quad planarity constraint has at most 12 non-zero entries.

Altogether, the infinitesimal rigidity matrix A is a sparse matrix and all entries of it can be explicitly expressed in terms of the vertex coordinates of the origami structure.

S2 Changing the geometry of the origami structure

It is noteworthy that the calculation of the infinitesimal rigidity matrix A involves the vertex coordinates of the Miura-ori structure. As discussed in [1], changing the geometric parameters of the Miura-ori structure, such as the angles γ and θ, does not affect the rigidity percolation. It is natural to further ask whether the explosive percolation transition will be affected by the geometry of the Miura-ori structure. To address this question, we changed the origami geometry and repeated the simulations with the two prescribed selection rules.

In Fig. S1(a), we show the geometry of Miura-ori structure used in the simulations in the main text (with the angle parameters $\gamma = \pi/4$ and $\theta = \cos^{-1}\sqrt{2/3}$) and the simulation results for $m = n = L = 10$ and $k = 1, 2, 4, 8, 16, 32$ based on the two selection rules. Then, we changed the angle parameters to be $\gamma = \pi/3$ and $\theta = \pi/3$ and repeated the simulations (500 simulations for each L and each k as in the main text). As shown in Fig. S1(b), the geometry of the Miura-ori structure is significantly different from the original one. Nevertheless, for both the Most Efficient selection rule and the Least Efficient selection rule, the simulation results are highly consistent with the ones obtained under the original setup. Specifically, it can be observed that increasing the number of choices k from 1 to 32 gives a highly similar trend in the increase of the sharpness of the transition of the probability P of getting a 1-DOF structure. In Fig. S1(c), we further considered another set of angle parameters $\gamma = \pi/6$ and $\theta = \pi/6$ for the Miura-ori geometry and repeated the simulations. Again, one can see that the simulation results are highly consistent with the above-mentioned ones.

From the above additional experiments, we conclude that the explosive rigidity percolation transition is independent of the geometry of the Miura-ori structure.

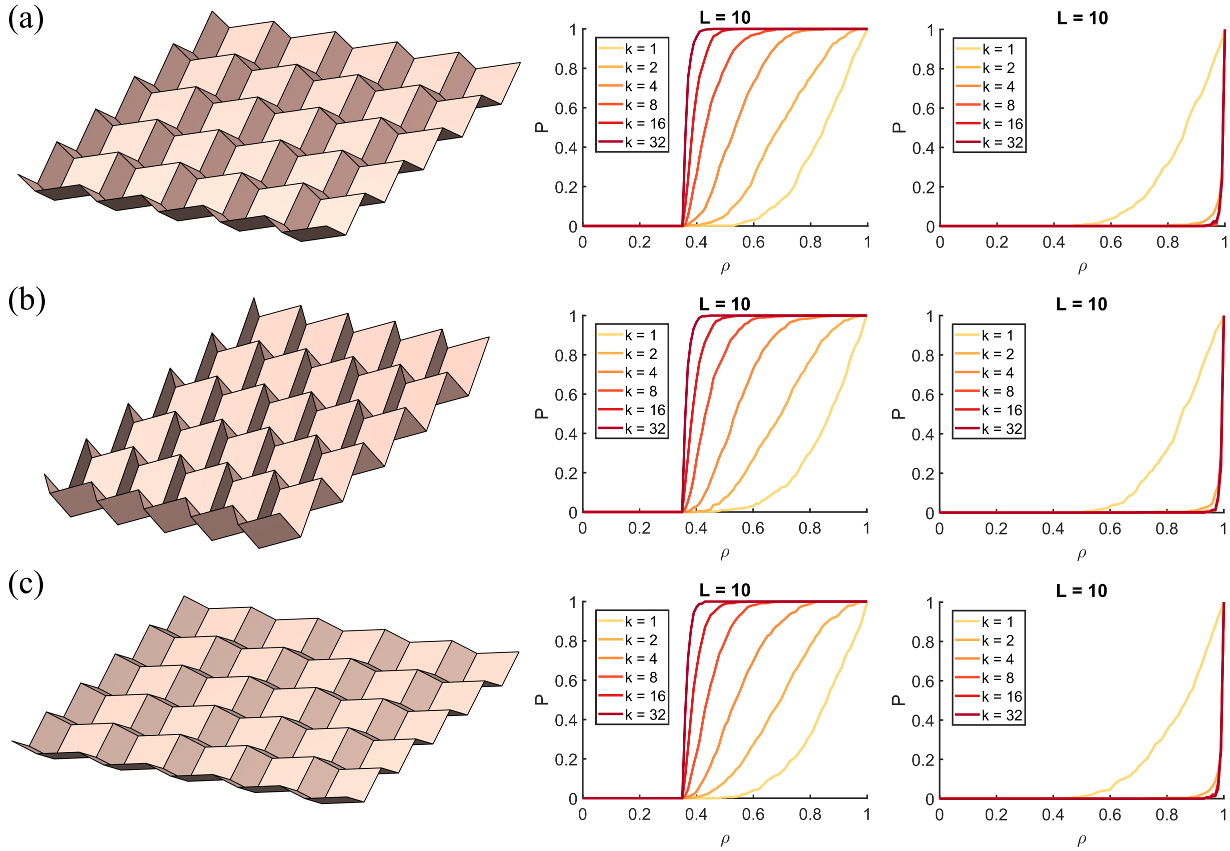

Figure S1: **Comparing the explosive rigidity percolation in origami with different geometric parameters.** (a) The results for $\gamma = \pi/4$ and $\theta = \cos^{-1}\sqrt{2/3}$. (b) The results for $\gamma = \pi/3$ and $\theta = \pi/3$. (c) The results for $\gamma = \pi/6$ and $\theta = \pi/6$. For each set of geometric parameters, we consider a 10×10 Miura-ori structure (left), the rigidity percolation simulation result based on the Most Efficient selection rule with different number of choices k, and the simulation result based on the Least Efficient rule (right). Here, ρ is the density of the planarity constraints explicitly imposed and P is the probability of getting a 1-DOF structure.

S3 Additional analysis of the square case

Note that in the main text, we presented the change in the normalized DOF $\widetilde{d}$ for different problem sizes and different selection rules. One can also visualize the change in the actual (unnormalized) DOF d as ρ increases. In Fig. S2, we show the change in d for $L = 5, 10, 15, 20, 25, 30$ and $k = 1, 2, 4, 8, 16, 32$ under different selection rules. Again, it can be observed that d decreases linearly at small ρ, which can be explained by the fact that adding each quad planarity constraint will lead to a change of 0 (redundant constraint) or -1 (effective constraint) in d, and most of the initial constraints are likely to be effective. The selection rule and the value of k then play an important role as ρ increases, leading to different sublinear regimes.

In the main text, we also studied the change in the rigidity percolation transition width in $L \times L$ Miura-ori under the Most Efficient selection rule as the number of choices k increases. In Table 1, we present the detailed statistics of the transition width for different pattern sizes $L \times L = 5 \times 5$, 10×10, 15×15, 20×20, 25×25, 30×30 and different number of choices $k = 1, 2, 4, 8, 16, 32$. Specifically, we record the values of ρ^a, defined as the maximum ρ with $P = a$, and ρ_b, defined as the minimum ρ with $P = b$, and the difference between them.

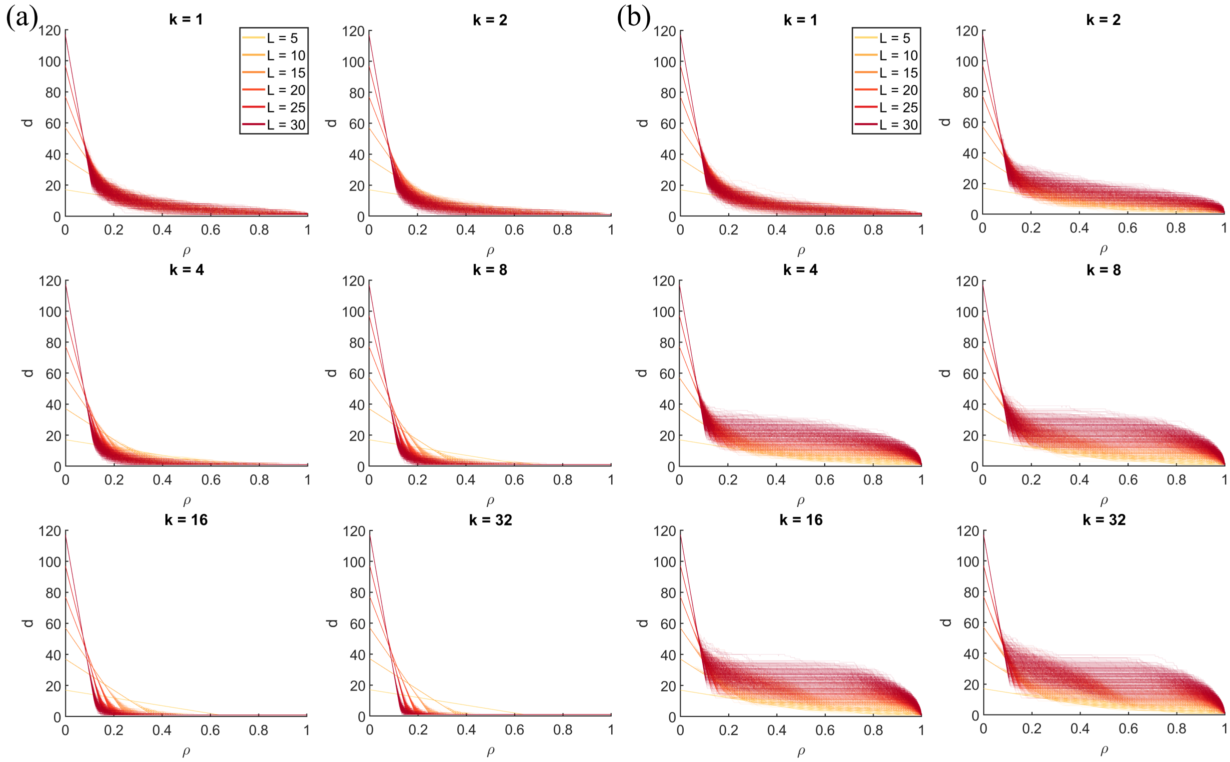

Figure S2: **The change in the actual DOF d under different selection rules with different number of choices for $L \times L$ Miura-ori structures.** (a) The Most Efficient selection rule. (b) The Least Efficient selection rule. For each $k = 1, 2, 4, 8, 16, 32$, we plot the actual DOF d in all 500 simulations for all $L = 5, 10, 15, 20, 25, 30$ on the same plot to visualize the change in $\widetilde{d}$. Each partially transparent curve represents one simulation, and the opacity is proportional to the number of repeated trends.

It can be observed from the table that both ρ^0 and ρ_1 decrease generally as k increases. However, their decreasing rates exhibit different behaviors. Specifically, for large pattern size $L \times L$, ρ^0 generally decreases faster than ρ_1 when the number of choices increases from $k = 1$ to some small k. This can also be visualized by plotting the simulated values of ρ^0 and ρ_1 as in Fig. S3(a)–(b), from which we can easily see that they show different decreasing rates. Also, as described in the main text, ρ^0 and ρ_1 can be fitted using two simple models involving a negative exponential term (main text Eq. (3.6) and Eq. (3.7)). In Fig. S3(c)–(d), we plot the fitted values of ρ^0 and ρ_1 for different pattern size L and number of choices k, from which we can easily see that both formulas match the simulation results very well. To further justify the formulation of the models, note that for $f(k, L) = r + s \exp\left(-ak^b/L^c\right)$ (where $a, b, c, r, s \geq 0$), the partial derivative $\frac{\partial f}{\partial k}$ decays to zero as $k \to \infty$, which is consistent with the observed saturation behavior. Also, the ratio k^b/L^c can capture the relative sampling intensity with respect to the origami pattern size, thereby naturally modelling diminishing returns when $k \gg L$. Therefore, we adopt this formulation in fitting both ρ^0 and ρ_1.

One may ask whether the above observations only hold for the transition interval between $P = 0$ and $P = 1$. Besides ρ^0 and ρ_1, here we also consider the difference between $\rho^{0.1}$ and $\rho_{0.9}$ (i.e. the transition width between $P = 0.1$ and $P = 0.9$) and the difference between $\rho^{0.25}$ and $\rho_{0.75}$ (i.e. the transition width between $P = 0.25$ and $P = 0.75$). As shown in Table 1, the differences for these transition intervals also show an increasing trend initially followed by a decreasing trend as k increases. This suggests that our analyses can be naturally extended to other transition intervals.

Pattern size ($L \times L$)	# choices (k)	ρ^0	ρ_1	$\rho_1 - \rho^0$	$\rho^{0.1}$	$\rho_{0.9}$	$\rho_{0.9} - \rho^{0.1}$	$\rho^{0.25}$	$\rho_{0.75}$	$\rho_{0.75} - \rho^{0.25}$
5×5	1	0.6000	1.0000	0.4000	0.6800	1.0000	0.3200	0.7600	0.9600	0.2000
	2	0.6000	0.9600	0.3600	0.6400	0.8800	0.2400	0.6800	0.8400	0.1600
	4	0.6000	0.8800	0.2800	0.6000	0.7600	0.1600	0.6000	0.7200	0.1200
	8	0.6000	0.7200	0.1200	0.6000	0.6800	0.0800	0.6000	0.6400	0.0400
	16	0.6000	0.6400	0.0400	0.6000	0.6400	0.0400	0.6000	0.6400	0.0400
	32	0.6000	0.6400	0.0400	0.6000	0.6400	0.0400	0.6000	0.6400	0.0400
10×10	1	0.4200	1.0000	0.5800	0.6700	0.9700	0.3000	0.7500	0.9300	0.1800
	2	0.3600	0.9700	0.6100	0.5300	0.8700	0.3400	0.6000	0.8000	0.2000
	4	0.3500	0.8600	0.5100	0.4300	0.6800	0.2500	0.4700	0.6100	0.1400
	8	0.3500	0.7100	0.3600	0.3700	0.5400	0.1700	0.3900	0.4900	0.1000
	16	0.3500	0.5500	0.2000	0.3500	0.4400	0.0900	0.3700	0.4100	0.0400
	32	0.3500	0.4600	0.1100	0.3500	0.3900	0.0400	0.3500	0.3700	0.0200
15×15	1	0.4178	1.0000	0.5822	0.6756	0.9778	0.3022	0.7644	0.9378	0.1733
	2	0.3244	0.9778	0.6533	0.4844	0.8667	0.3822	0.5733	0.7911	0.2178
	4	0.2933	0.8978	0.6044	0.3644	0.6622	0.2978	0.4222	0.5822	0.1600
	8	0.2444	0.6711	0.4267	0.2933	0.5022	0.2089	0.3200	0.4311	0.1111
	16	0.2489	0.4800	0.2311	0.2667	0.3689	0.1022	0.2800	0.3378	0.0578
	32	0.2444	0.4000	0.1556	0.2489	0.3022	0.0533	0.2533	0.2844	0.0311
20×20	1	0.3250	1.0000	0.6750	0.6550	0.9825	0.3275	0.7475	0.9400	0.1925
	2	0.3250	0.9825	0.6575	0.4775	0.8475	0.3700	0.5550	0.7600	0.2050
	4	0.2400	0.8925	0.6525	0.3375	0.6650	0.3275	0.3950	0.5750	0.1800
	8	0.2100	0.7025	0.4925	0.2575	0.4625	0.2050	0.2825	0.4025	0.1200
	16	0.1950	0.5325	0.3375	0.2200	0.3325	0.1125	0.2325	0.2900	0.0575
	32	0.1875	0.3150	0.1275	0.1975	0.2625	0.0650	0.2050	0.2400	0.0350
25×25	1	0.4400	1.0000	0.5600	0.6832	0.9696	0.2864	0.7824	0.9328	0.1504
	2	0.3040	0.9648	0.6608	0.4672	0.8432	0.3760	0.5552	0.7632	0.2080
	4	0.2448	0.8816	0.6368	0.3216	0.6144	0.2928	0.3744	0.5216	0.1472
	8	0.1776	0.7328	0.5552	0.2336	0.4640	0.2304	0.2640	0.3936	0.1296
	16	0.1600	0.4512	0.2912	0.1888	0.3024	0.1136	0.2048	0.2672	0.0624
	32	0.1536	0.3200	0.1664	0.1680	0.2288	0.0608	0.1760	0.2080	0.0320
30×30	1	0.4044	0.9989	0.5944	0.6722	0.9756	0.3033	0.7678	0.9367	0.1689
	2	0.2689	0.9700	0.7011	0.4500	0.8656	0.4156	0.5300	0.7600	0.2300
	4	0.2089	0.9633	0.7544	0.2967	0.6333	0.3367	0.3600	0.5411	0.1811
	8	0.1600	0.6622	0.5022	0.2178	0.4300	0.2122	0.2478	0.3700	0.1222
	16	0.1444	0.4656	0.3211	0.1700	0.2856	0.1156	0.1867	0.2422	0.0556
	32	0.1300	0.3133	0.1833	0.1467	0.2178	0.0711	0.1544	0.1933	0.0389

Table 1: **Experimental transition values of the probability of getting a 1-DOF $L \times L$ Miura-ori structure under the Most Efficient selection rule.** For each pattern size L, we run 500 simulations with an $L \times L$ Miura-ori pattern and calculate the probability P of getting a 1-DOF structure. We then define ρ^a as the maximum ρ with $P = a$ and ρ_b as the minimum ρ with $P = b$ and record their values for different a, b for different number of choices k. The difference between every pair of values is also recorded.

S4 Additional analysis of the general rectangular case

In Eq. (3.10) in the main text, we gave a simple quadratic model for describing the difference between the critical transition density and the theoretical minimum density $\rho_{\text{diff}} = \rho^* - \rho_{\min}$ for general $m \times n$ Miura-ori structures with different number of choices under the Most Efficient selection rule. In Fig. S4, we provide additional examples with $mn = 36, 64, 100, 144, 196$. It can be observed that the simulated ρ_{diff} is highly symmetric in all examples. Also, we can easily see that the fitted values of ρ_{diff} using our proposed model match the simulation results very well.

Also, we proposed a simple approximation formula for the rigidity percolation transition width ρ_w for any given (m, n, k) for general $m \times n$ Miura-ori structures in the main text. In Fig. S5, we provide additional examples with $mn = 36, 64, 100, 144, 196$ for visualizing the change of ρ_w with different combinations of (m, n, k). Again, we can see that the fitted ρ_w using our proposed model largely resembles the simulated transition width for all mn.

Besides, as ρ_w is roughly symmetric about $\log(m/n) = 0$, it is natural to ask whether one can also

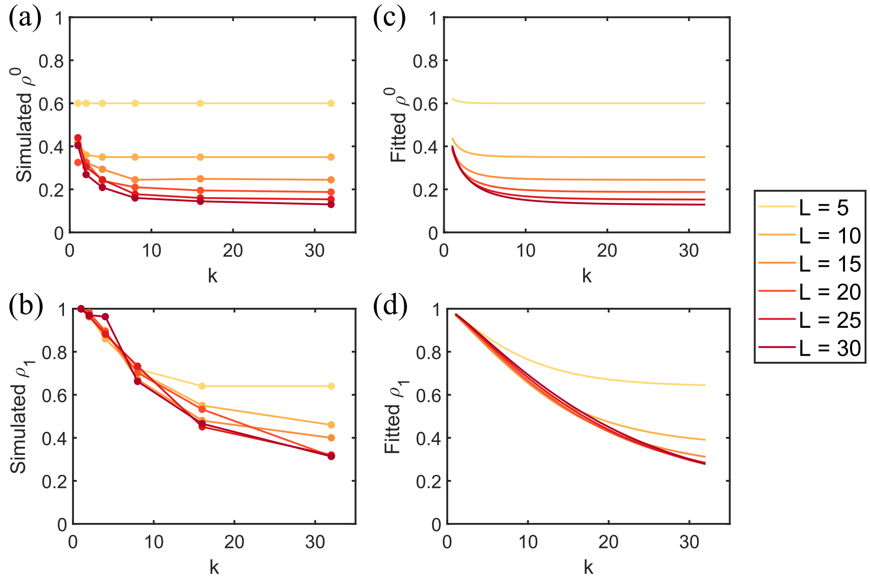

Figure S3: **The simulated and fitted ρ^0 and ρ_1 for $L \times L$ Miura-ori structures under the Most Efficient selection rule.** (a)–(b) The simulated ρ^0 and ρ_1, where each data point represents the result obtained from 500 simulations for a given set of parameters (L, k) (with $L = 5, 10, 15, 20, 25, 30$ and $k = 1, 2, 4, 8, 16, 32$). (c)–(d) The fitted ρ^0 and ρ_1 obtained using the proposed models in Eq. (3.6) and Eq. (3.7) in the main text.

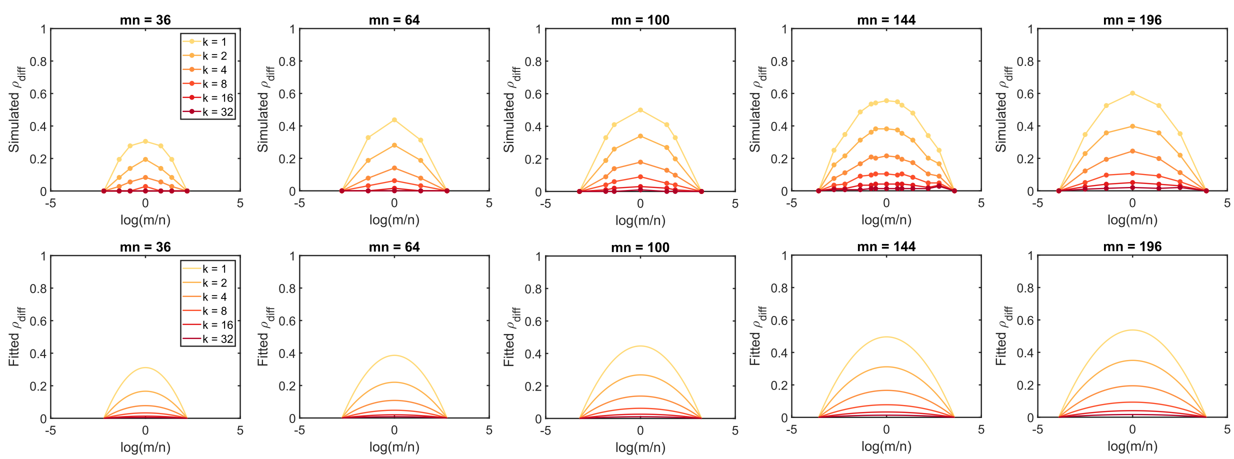

Figure S4: **The simulated and fitted $\rho_{\text{diff}} = \rho^* - \rho_{\min}$ for general $m \times n$ Miura-ori structures under the Most Efficient selection rule.** The first row shows the simulation results for $mn = 36, 64, 100, 144, 196$, where each data point represents the result obtained from 500 simulations for a specific combination (m, n, k) with $k = 1, 2, 4, 8, 16, 32$. The second row shows the fitted values of ρ_{diff} using our proposed model in Eq. (3.10) in the main text.

approximate ρ_w using a simple quadratic polynomial in $\log(m/n)$ analogous to the one for ρ_{diff} in the main text. Here, we consider the following alternative approximation formula for ρ_w:

$$\rho_w(m, n, k) \approx \left(\rho_w(L, k) - \frac{1}{mn}\right)\left(1 - \left(\frac{\log(m/n)}{\log(mn/4)}\right)^2\right) + \frac{1}{mn}, \tag{S16}$$

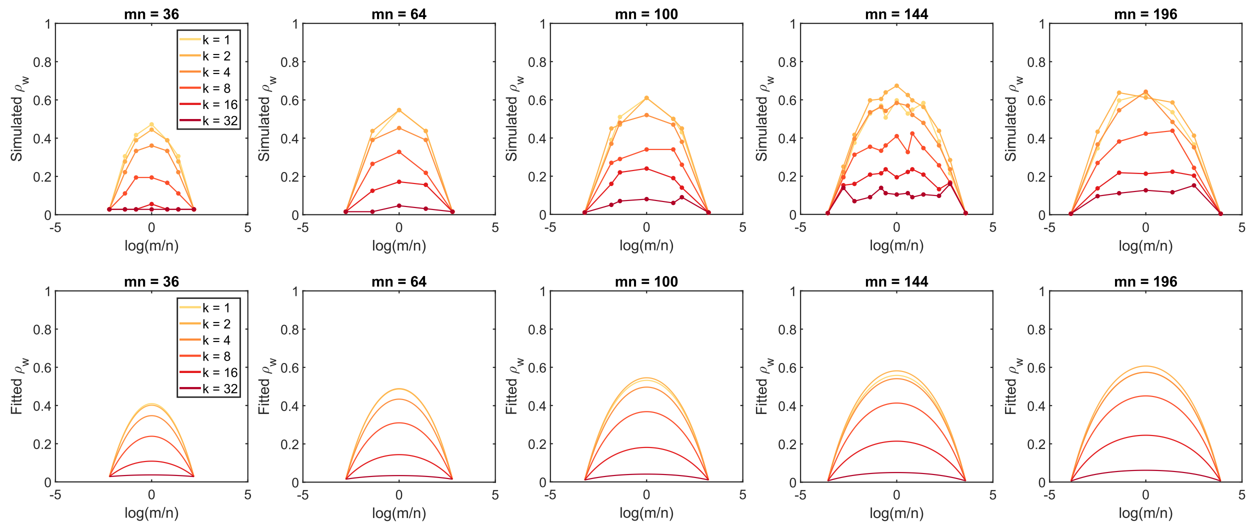

Figure S5: **The simulated and fitted rigidity percolation transition width ρ_w for general $m \times n$ Miura-ori structures under the Most Efficient selection rule.** The first row shows the simulation results for $mn = 36, 64, 100, 144, 196$, where each data point represents the result obtained from 500 simulations for a specific combination (m, n, k) with $k = 1, 2, 4, 8, 16, 32$. The second row shows the fitted values of ρ_w using our proposed model.

where $\rho_w(L, k)$ is the fitted value for the square case $L \times L$ with $L = \sqrt{mn}$ using main text Eq. (3.8). Specifically, note that for $m = n$, we have $\log(m/n) = 0$ and hence

$$\left(\rho_w(L,k) - \frac{1}{mn}\right)(1-0)^2 + \frac{1}{mn} = \rho_w(L,k). \tag{S17}$$

In other words, Eq. (S16) is identical to Eq. (3.8) in the main text if $m = n$. Also, it is easy to see that Eq. (S16) is perfectly symmetric and gives the same value for (m, n, k) and (n, m, k), which matches our observation. Moreover, for the extreme case where $m = 2$ or $n = 2$, note that all facets of the Miura-ori structure are boundary facets and we need to explicitly add the quad planarity constraints to all of them to make the structure 1-DOF. This requires exactly mn steps and hence the theoretical transition width will be $1/(mn)$. Now, if $n = 2$, we have

$$1 - \left(\frac{\log(m/n)}{\log(mn/4)}\right)^2 = 1 - \left(\frac{\log((mn/2)/2)}{\log(mn/4)}\right)^2 = 1 - 1 = 0, \tag{S18}$$

and it follows from Eq. (S16) that

$$\rho_w \approx 0 + \frac{1}{mn} = \frac{1}{mn}. \tag{S19}$$

Similarly, if $m = 2$, we have $\rho_w \approx 1/(mn)$. This shows that Eq. (S16) matches the expected ρ_w at the peak and the two endpoints. In Fig. S6, we compare the fitted values of ρ_w by this simple quadratic model and the simulation results for different combinations of (m, n, k) as in the main text. It can be observed that this alternative model gives a qualitatively good fit, with most data points being close to the line $y = x$. However, comparing this plot with the plot for the original model in main text Fig. 10(c), we can see that the original model in main text Eq. (3.12) gives a better fit with a smaller deviation from $y = x$.

Altogether, this alternative model provides a simple and reasonably accurate way to connect the rigidity percolation transition width of $L \times L$ Miura-ori structures with that of all other Miura-ori structures with the same total number of facets.

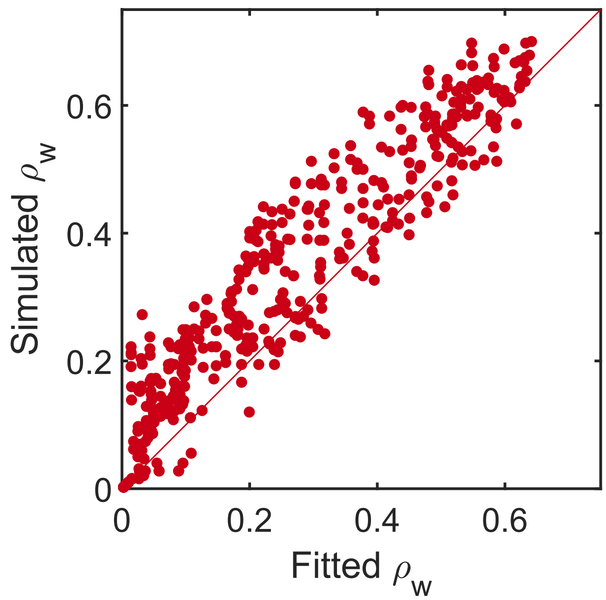

Figure S6: **A comparison between the simulated rigidity percolation transition width ρ_w and the alternative model in Eq. (S16) for $m \times n$ Miura-ori structures.** Each data point represents the fitted value (x-coordinate) and simulated value (y-coordinate) for a combination of (m, n, k), with $mn = 25, 36, 49, 64, \ldots, 400$ and $k = 1, 2, 4, 8, 16, 32$. The red line represents $y = x$.

References

[1] S. Chen and L. Mahadevan, "Rigidity percolation and geometric information in floppy origami," *Proc. Natl. Acad. Sci.*, vol. 116, no. 17, pp. 8119–8124, 2019.